Iranian Journal of Materials Forming 7 (2) (2020) 2-7

Online ISSN: 2383-0042

IJMF

Iranian Journal of Materials Forming

Journal Homepage: http://ijmf.shirazu.ac.ir

Research Article

Controlling the Mechanical Properties and Corrosion Resistance of Mild Steel by Intercritical Annealing and Subcritical Tempering

M. Soleimani, H. Mirzadeh* and Ch. Dehghanian

School of Metallurgy and Materials Engineering, College of Engineering, University of Tehran, Tehran, Iran

ARTICLE INFO

Article history:

Received 7 March 2020
Revised 6 April 2020
Accepted 11 April 2020

Keywords:

Mild steel
Intercritical annealing
Subcritical tempering
Mechanical properties
Corrosion resistance

ABSTRACT

The effects of intercritical annealing and subcritical tempering on the mechanical properties and corrosion resistance of mild steel were studied. It was revealed that intercritical annealing followed by quenching resulted in the development of a ferritic-martensitic dual phase (DP) microstructure with high tensile strength, disappearance of the yield-point phenomenon, superior work-hardening behavior, and decreased corrosion resistance. Subsequent tempering of the intercritically annealed steel resulted in the formation of carbide particles in a tempered martensitic microstructure, which led to the decline of the strength and hardness, reappearance of the yield-point elongation, and enhanced corrosion resistance. Accordingly, this work demonstrated the possibility of controlling the mechanical properties and corrosion resistance of commercial mild steels by simple heat treatments.

1. Introduction

Adjusting the chemical composition [1], intercritical annealing [2-5], grain refinement [6-11], bake hardening [12-14], and tempering treatment [15-19] are among the main routes for controlling the mechanical properties of mild steel.

The intercritical annealing followed by water quenching is usually used to process ferritic-martensitic steels known as dual phase (DP) steels, which show improved work-hardening behavior and superior strength-ductility balance [20-22]. While the steel is usually a low carbon type, the martensite phase in the intercritically annealed steels might be high carbon, which is related to the presence of the majority of carbon content of the steel in the martensite phase with low fraction (10 to 40 vol%) [23]. Therefore, the tempering treatment of intercritically annealed steels is usually used to enhance plasticity [17]. The presence of martensite is also known to impair the corrosion resistance of mild steel [24-26], where the tempering treatment might be also advantageous in this regard.

However, understanding the effects of intercritical annealing and tempering treatment on the corrosion resistance of mild steel need more experimental works. In response, the effects of intercritical annealing and tempering treatment on the microstructure, hardness, tensile properties, and corrosion resistance of a commercial mild steel has been studied in the present work.

2. Experimental Details

2.1. Processing

A common mild steel (st37 grade) with the chemical composition (wt%) of 0.12C-1.11Mn-0.16Si was received in the fully annealed condition. As shown in Fig. 1, the as-received sample had a ferritic-pearlitic microstructure and the average ferrite grain size was ~ 46 μm. A cylindrical specimen with the diameter of 2 mm and length of 10 mm was heated up to 1000°C at the

* Corresponding author
E-mail address: hmirzadeh@ut.ac.ir (H. Mirzadeh)

rate of 2°C/s in a dilatometer, and as shown in Fig. 1, the Ac_1 and Ac_3 temperatures were determined by dilatometry as 730°C and 904°C, respectively. The as-received sample was intercritically annealed at 850°C for holding times up to 20 min, which was followed by water quenching to develop the ferritic-martensitic DP steel. The intercritically annealed sample for 15 min was then tempered at 600°C for tempering times up to 360 min.

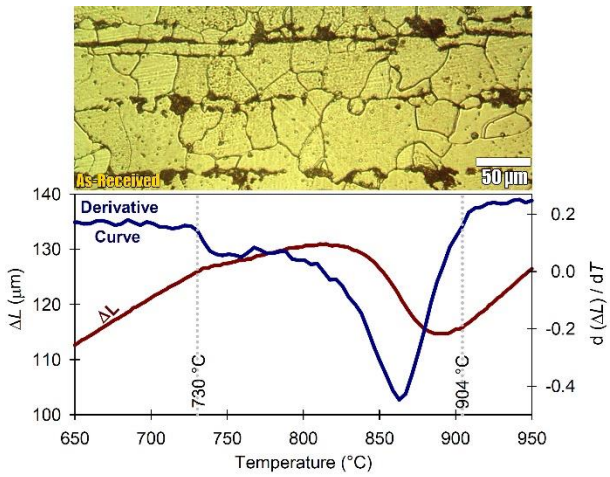

Fig. 1. As-received microstructure and its dilatometric curve.

2.2. Characterization

An optical microscope and a FEI Nova field-emission SEM were used for microstructural characterization. The samples were etched by the LePera's reagent / 2% Nital solution. Vickers hardness test (load of 5 kg) was used for studying the austenitization during intercritical annealing and the subsequent tempering process.

The subsize ASTM E8 samples were tensile tested at room temperature under a constant cross-head speed of 1 mm/min, where each test was repeated once to ensure the reproducibility of the results. The work-hardening rate was obtained based on $\theta = d\sigma/d\varepsilon = \{\sigma_{i+1}-\sigma_{i+1}\}/\{\varepsilon_{i+1}-\varepsilon_{i+1}\}$ [27]. Moreover, according to the Hollomon equation and the Considére criterion ($\theta = \sigma$ at the point of instability in tension), the work-hardening exponent (n) becomes equal to the uniform true strain (ε_u) [28].

The polarization tests in a 3.5 wt% NaCl solution at room temperature were performed using a Solartron potentiostat (Model SI 1287) operating at the scanning speed of 2 mV/s. The specimen surface was ground and polished and an area of 1 cm^2 was exposed to the solution for each sample. These tests were repeated twice for statistical analysis.

3. Results and Discussion

3.1. Microstructural evolutions

Figure 2 shows the variation of hardness during intercritical annealing up to holding times of 20 min. By increasing the holding time, the hardness was increased, which was related to the partial austenitization during intercritical annealing and subsequent transformation of austenite to martensite during water quenching from the intercritical annealing temperature. The hardness eventually saturates at ~ 15 min and reaches a plateau as shown in Fig. 2. Therefore, the intercritically annealed sample for 15 min (IA15 sample) was considered as the representative of the developed DP steel. The microstructure of this sample is shown in Fig. 3(a), where this optical micrograph reveals the presence of martensite islands in a matrix of ferrite. The SEM image of this sample in Fig. 3(b) shows the morphology of the martensite phase at high magnification.

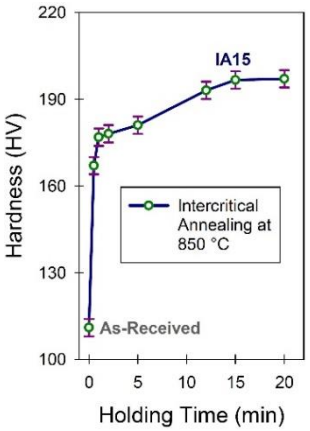

Fig. 2. Evolutions of hardness during intercritical annealing of the as-received sample.

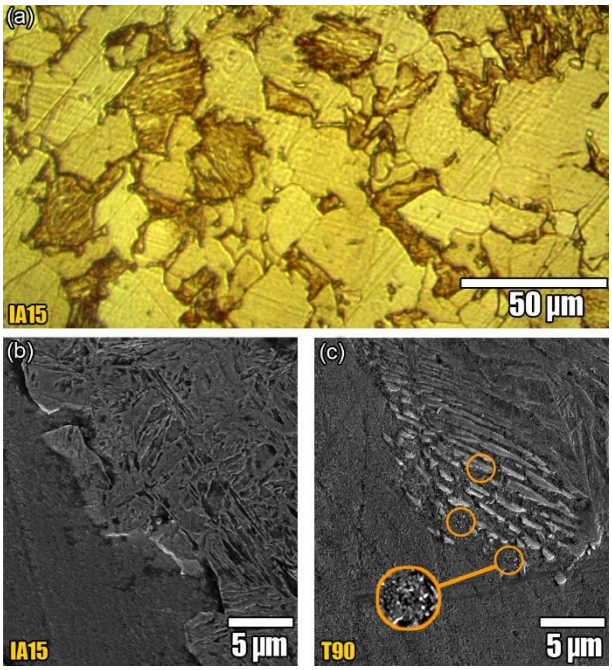

Fig. 3. Representative microstructures of a) and b) IA15 and (c) T90 samples.

Figure 4 depicts the variation of hardness during tempering of the IA15 sample at 600 °C for tempering times up to 360 min. It can be seen that during tempering, the hardness was decreased, and reached a plateau at long holding times. The SEM image of the sample tempered for 90 min (T90 sample) is shown in Fig. 3(c), where the formation of nanometric carbide particles and tendency for vanishing of the lath martensitic morphology is evident. The microstructure of the sample tempered for 360 min (T360 sample) was comparable to that of T90 sample, except the more intense tempering effects in the former. These observations are responsible for the decline of hardness during tempering of IA15 sample. In fact, tempering of a martensitic microstructure mainly involves the precipitation of transition carbides (and the lowering of the carbon content of the martensitic matrix) and the replacement of the transition carbide and low-carbon martensite by cementite and ferrite [29]. Similarly, during tempering, in the martensitic islands of DP steel, the same phenomena happen as shown by Mazinani and Poole [15], Waterschoot and Verbeken [16], Fonstein et al. [17], Han et al. [18], Li et al. [19].

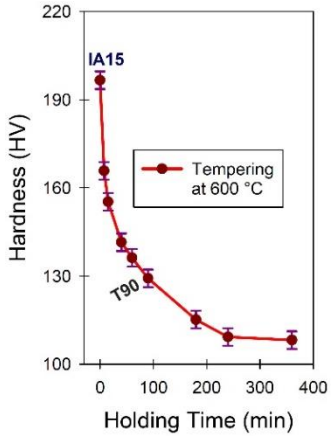

Fig. 4. Evolutions of hardness during tempering of the IA15 sample.

3.2. Tensile properties

Figure 5 depicts the tensile stress-strain curves of as-received and IA15 samples. The ultimate tensile strength (UTS) of IA15 sample is higher than that of the as-received sample due to the replacement of pearlite and some fraction of ferrite in the as-received sample with martensite in the IA15 sample. The tensile curves also revealed the superior work hardening behavior of the IA15 sample when compared to that of the as-received sample. This effect is shown in Fig. 6 based on the work-hardening analysis according to the Crussard–Jaoul method [4, 20, 30], where the work hardening rate of IA15 sample is higher at each considered true strain. Moreover, based on Fig. 5, the IA15 sample does not show the yield-point phenomenon while this effect can be seen for the as-received sample. The yield-point phenomenon resulted in the low initial work-hardening rates for the as-received sample in Fig. 6. The absence of the yield-point phenomenon in the former is related to the formation of quench-induced dislocations in ferrite around the martensite islands [3, 31], and hence, the presence of free dislocations during subsequent tensile testing.

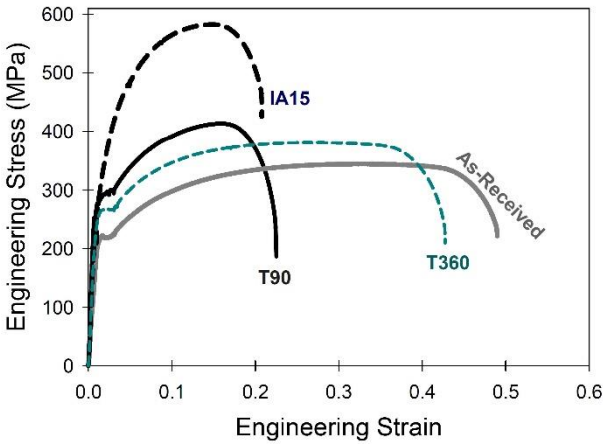

Fig. 5. Tensile stress-strain curves.

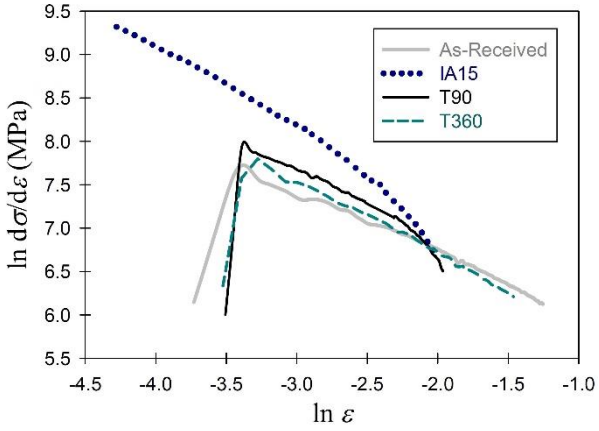

Fig. 6. Work-hardening rate plots based on the true stress-strain curves, where the data has been cut off at the UTS of the engineering stress-strain curves.

Figure 5 also shows the tensile stress-strain curve of the T90 sample. It can be seen that this sample shows the yield-point phenomenon, which is related to the tempering effects as also confirmed by Gündüz [32]. Moreover, the UTS of this sample is lower than that of IA15 sample but it is higher than that of the as-received sample. Moreover, the stress-strain curve of the T360 sample shows decreased strength but increased ductility as expected based on the trend of hardness in Fig. 4. These results reveal that by controlling the tempering time, it is possible to alter the mechanical properties. The corresponding work-hardening plots in Fig. 6 reveal the

decline in the work-hardening rate but also show an increase in the work-hardening exponent (*n*-value) from 0.132 ($\ln\varepsilon_{uniform} = -2.02$) for the IA15 sample to 0.145 ($\ln\varepsilon_{uniform} = -1.93$) for the T90 sample and 0.232 ($\ln\varepsilon_{uniform} = -1.46$) for the T360 sample. Therefore, the uniform true strain, and hence, the uniform elongation increased by tempering treatment.

3.3. Corrosion resistance

The polarization curves of the samples are shown in Fig. 7(a), where the values of corrosion current density (i_{corr}) were determined based on the Tafel extrapolation method [33, 34]. The obtained values of i_{corr} are shown in the bar chart of Fig. 7(b). It can be seen that the i_{corr} for the IA15 sample is much larger than that determined for the as-received sample. This reveals that the substitution of pearlite and the surrounding ferrite with martensite impairs the corrosion resistance, which is consistent with the works of Soleimani et al. [24], Kayali and Anaturk [25], Allam and Abbas [26], and Keleştemur et al. [35]. It can be also seen that tempering enhances the corrosion resistance and the i_{corr} for the T90 sample is much smaller than that determined for the IA15 sample. This seems to be inconsistent with the work of Keleştemur et al. [35], where the corrosion rate of the dual-phase steel embedded in concrete increased with tempering heat treatment and the highest corrosion rate took place in dual-phase steel tempered at 300°C. However, in the present work, the tempering temperature of 600°C was used, which can explain the enhanced corrosion resistance. This work clearly shows that the tempering treatment can be applied to the intercritically annealed mild steel to enhance its corrosion resistance.

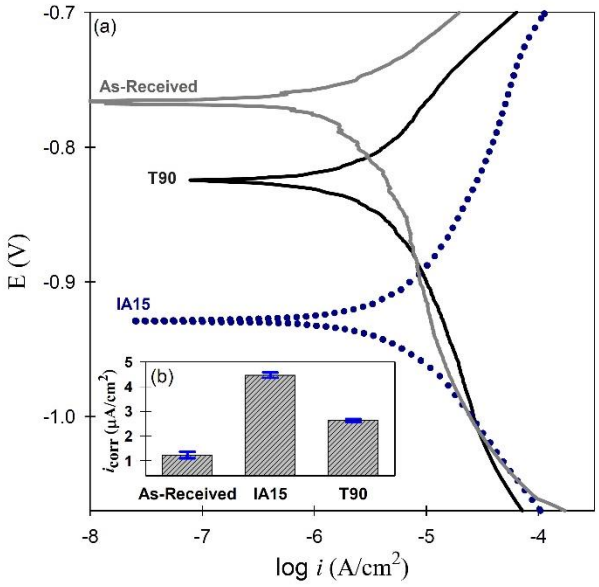

Fig. 7. (a) Polarization curves and (b) the obtained values of the corrosion current density for the processed samples.

4. Conclusions

The mechanical properties and corrosion resistance of mild steel as influenced by the intercritical annealing and subcritical tempering were studied. It was revealed that intercritical annealing followed by quenching resulted in the development of DP microstructure with high tensile strength, disappearance of the yield-point phenomenon, superior work-hardening behavior, and poor corrosion resistance. Subsequent tempering of the intercritically annealed steel resulted in the formation of carbide particles in a tempered martensitic microstructure. Accordingly, during tempering, the hardness decreased until reaching a plateau. This decrease, in turn, led to the decline of the strength and hardness, reappearance of the yield-point elongation, and enhanced corrosion resistance. Conclusively, this work demonstrated the possibility of controlling the mechanical properties and corrosion resistance of commercial mild steels by simple heat treatments.

5. References

[1] Z. Nasiri, S. Ghaemifar, M. Naghizadeh, H. Mirzadeh, Thermal mechanisms of grain refinement in steels: A review, *Metals and Materials International*, in press, (2020) DOI: 10.1007/s12540-020-00700-1.

[2] J. Zhang, H. Di, Y. Deng, R.D.K. Misra, Effect of martensite morphology and volume fraction on strain hardening and fracture behavior of martensite–ferrite dual phase steel, *Materials Science and Engineering A* 627 (2015) 230-240.

[3] M. Nouroozi, H. Mirzadeh, M. Zamani, Effect of microstructural refinement and intercritical annealing time on mechanical properties of high-formability dual phase steel, *Materials Science and Engineering A* 736 (2018) 22-26.

[4] D. Das, P.P. Chattopadhyay, Influence of martensite morphology on the work-hardening behavior of high strength ferrite–martensite dual-phase steel, *Journal of Materials Science* 44 (2009) 2957-2965.

[5] S. Nikkhah, H. Mirzadeh, M. Zamani, Fine tuning the mechanical properties of dual phase steel via thermomechanical processing of cold rolling and intercritical annealing, *Materials Chemistry and Physics* 230 (2019) 1-8.

[6] H. Azizi-Alizamini, M. Militzer, and W.J. Poole, Formation of ultrafine grained dual phase steels through rapid heating, *ISIJ International* 51 (2011) 958-964.

[7] A.H. Jahanara, Y. Mazaheri, M. Sheikhi, Correlation of ferrite and martensite micromechanical behavior with mechanical properties of ultrafine grained dual phase steels, *Materials Science and Engineering A* 764 (2019) 138206.

[8] M. Soleimani, H. Mirzadeh, C. Dehghanian, Effect of grain size on the corrosion resistance of low carbon steel, *Materials Research Express* 7 (2020) 016522.

[9] M. Calcagnotto, D. Ponge, and D. Raabe, Effect of grain refinement to 1 μm on strength and toughness of dual-phase steels, *Materials Science and Engineering A* 527 (2010) 7832-7840.

[10] N. Nakada, Y. Arakawa, K.S. Park, T. Tsuchiyama, S. Takaki, Dual phase structure formed by partial reversion of cold-deformed martensite, *Materials Science and Engineering A* 553 (2012) 128-133.

[11] Y.G. Deng, Y. Li, H. Di, R.D.K. Misra, Effect of Heating Rate during Continuous Annealing on Microstructure and Mechanical Properties of High-Strength Dual-Phase Steel, *Journal of Materials Engineering and Performance* 28 (2019) 4556-4564.

[12] N. Ormsuptave, V. Uthaisangsuk, Modeling of bake-hardening effect for fine grain bainite-aided dual phase steel, *Materials and Design* 118 (2017) 314-329.

[13] A. Ramazani, S. Bruehl, T. Gerber, W. Bleck, U. Prahl, Quantification of bake hardening effect in DP600 and TRIP700 steels, *Materials and Design* 57 (2014) 479-486.

[14] N. Ormsuptave, V. Uthaisangsuk, Effect of fine grained dual phase steel on bake hardening properties, *Steel Research International* 88 (2017) 1600150.

[15] M. Mazinani, W.J. Poole, Effect of martensite plasticity on the deformation behavior of a low-carbon dual-phase steel, *Metallurgical and materials transactions A* 38 (2007) 328-339.

[16] T. Waterschoot, K. Verbeken, Tempering kinetics of the martensitic phase in DP steel, *ISIJ international* 46 (2006) 138-146.

[17] N. Fonstein, M. Kapustin, N. Pottore, I. Gupta, O. Yakubovsky, Factors that determine the level of the yield strength and the return of the yield-point elongation in low-alloy ferrite-martensite steels, *The Physics of Metals and Metallography* 104 (2007) 315-323.

[18] Q. Han, A. Asgari, P.D. Hodgson, N. Stanford, Strain partitioning in dual-phase steels containing tempered martensite, *Materials Science and Engineering A* 611 (2014) 90-99.

[19] H. Li, S. Gao, Y. Tian, D. Terada, A. Shibata, N. Tsuji, Influence of tempering on mechanical properties of ferrite and martensite dual phase steel, *Materials Today: Proceedings* 2 (2015) S667-S671.

[20] H. Mirzadeh, M. Alibeyki, M. Najafi, Unraveling the initial microstructure effects on mechanical properties and work-hardening capacity of dual phase steel, *Metallurgical and Materials Transactions A* 48 (2017) 4565-4573.

[21] B. Gao, X. Chen, Z. Pan, J. Li, Y. Ma, Y. Cao, M. Liu, Q. Lai, L. Xiao, H. Zhou, A high-strength heterogeneous structural dual-phase steel, *Journal of Materials Science* 54 (2019) 12898-12910.

[22] T. Dutta, S. Dey, S. Datta, D. Das, Designing dual-phase steels with improved performance using ANN and GA in tandem, *Computational Materials Science* 157 (2019) 6-16.

[23] M. Alibeyki, H. Mirzadeh, M. Najafi, A. Kalhor, Modification of Rule of Mixtures for Estimation of the Mechanical Properties of Dual-Phase Steel, *Journal of Materials Engineering and Performance* 26 (2017) 2683-2688.

[24] M. Soleimani, H. Mirzadeh, C. Dehghanian, Unraveling the Effect of Martensite Volume Fraction on the Mechanical and Corrosion Properties of Low Carbon Dual Phase Steel, *Steel Research International* 91 (2020) 1900327.

[25] Y. Kayali, B. Anaturk, Investigation of electrochemical corrosion behavior in a 3.5 wt.% NaCl solution of boronized dual-phase steel, *Materials and Design* 46 (2013) 776-783.

[26] T. Allam, M. Abbas, Mechanical Properties, Formability, and Corrosion Behavior of Dual Phase Weathering Steels Developed by an Intercritical Annealing Treatment, *Steel Research International* 86 (2015) 231-240.

[27] S. Saadatkia, H. Mirzadeh, J.M. Cabrera, Hot deformation behavior, dynamic recrystallization, and physically-based constitutive modeling of plain carbon steels, *Materials Science and Engineering* A 636 (2015) 196-202.

[28] G.E. Dieter, Mechanical Metallurgy, third ed., McGraw-Hill, 1988.

[29] G. Krauss, Tempering of lath martensite in low and medium carbon steels: assessment and challenges, *Steel Research International* 88 (2017) 1700038.

[30] A. Bag, K.K. Ray, E.S. Dwarakadasa, Influence of martensite content and morphology on tensile and impact properties of high-martensite dual-phase steels, *Metallurgical and Materials Transactions A* 30 (1999) 1193-1202.

[31] G. Krauss, Steels processing, structure, and performance, 2nd ed, ASM International, 2015.

[32] S. Gündüz, Effect of chemical composition, martensite volume fraction and tempering on tensile behaviour of dual phase steels, *Materials letters* 63 (2009) 2381-2383.

[33] Y.C. Lin, G. Liu, M.S. Chen, J.L. Zhang, Z.G. Chen, Y.Q. Jiang, J. Li, Corrosion resistance of a two-stage stress-aged Al–Cu–Mg alloy: Effects of external stress, *Journal of Alloys and Compounds* 661 (2016) 221-230.

[34] Y.C. Lin, G. Liu, M.S. Chen, Y.C. Huang, Z.G. Chen, X. Ma, Y.Q. Jiang, J. Li, Corrosion resistance of a two-stage stress-aged Al–Cu–Mg alloy: Effects of stress-aging temperature, *Journal of Alloys and Compounds* 657 (2016) 855-865.

[35] O. Keleştemur, M. Aksoy, S. Yildiz, Corrosion behavior of tempered dual-phase steel embedded in concrete, International Journal of Minerals, *Metallurgy and Materials* 16 (2009) 43-50.

کنترل خواص مکانیکی و مقاومت به خوردگی فولاد کربنی توسط آنیل بین بحرانی و بازپخت در دمای زیر بحرانی

مریم سلیمانی، حامد میرزاده و چنگیز دهقانیان

دانشکده مهندسی متالورژی و مواد، دانشکده فنی، دانشگاه تهران، تهران، ایران.

چکیـــده

تاثیر آنیل بین بحرانی و بازپخت در دمای زیر بحرانی بر خواص مکانیکی و مقاومت به خوردگی فولاد کربنی بررسی شد. آنیل بین بحرانی و کوئنچ پس از آن منجر به توسعه ریزساختار دوفازی فریتی-مارتنزیتی با استحکام کششی بالا، عدم مشاهده پدیده نقطه تسلیم، رفتار کارسختی عالی، و کاهش مقاومت به خوردگی شد. در ادامه، بازپخت در دمای زیر بحرانی منجر به تشکیل ذرات کاربیدی در ریزساختار مارتنزیت تمپر شده شد که با کاهش استحکام و سختی، بازگشت پدیده نقطه تسلیم، و بهبود مقاومت به خوردگی همراه بود. در نتیجه، این تحقیق نشان داد که امکان کنترل خواص مکانیکی و مقاومت به خوردگی فولادهای کربنی تجاری با عملیات حرارتی ساده وجود دارد.

واژه‌های کلیدی: فولاد کربنی، آنیل بین بحرانی، بازپخت در دمای زیر بحرانی، خواص مکانیکی، مقاومت به خوردگی